Optical trapping performance of circular Pearcey beams on Mie particles

Xiaofang Lu,[1] Liu Tan,[1] Nana Liu,[1] Chuanwen Chen,[1] Kaijian Chen,[1] Haixia Wu,[1] Xiaoshuang Xia,[1] Peiyu Zhang,[1] Peilong Hong,[2,3] Bingsuo Zou,[4] and Yi Liang[1,3,5,*]

[1]*Guangxi Key Laboratory for Relativistic Astrophysics, Center on Nanoenergy Research, Guangxi Colleges and Universities Key Laboratory of Blue Energy and Systems Integration, School of Physical Science and Technology, Guangxi University, Nanning, Guangxi 530004, China*

[2]*School of Mathematics and Physics, Anqing Normal University, Anqing, Anhui 246133, China*

[3]*The MOE Key Laboratory of Weak-Light Nonlinear Photonics, TEDA Applied Physics Institute and School of Physics, Nankai University, Tianjin 300457, China*

[4]*School of Physical Science and Technology and School of Resources, Environment and Materials, Key Laboratory of New Processing Technology for Nonferrous Metals and Materials, Guangxi University, Nanning 530004, China*

[5]*State Key Laboratory of Featured Metal Materials and Life-cycle Safety for Composite Structures, Nanning 530004, China*

(Received 28 August 2023; accepted 30 November 2023; published 18 December 2023)

We focused on investigating the trapping characteristics of the circular Pearcey beam (CPB) on Mie particles. To study the trapping performance of CPB on particles of different sizes, we employed the generalized Lorenz-Mie theory (GLMT) for analysis. Our results revealed that the CPB exhibits a stronger optical trapping force for a larger Mie particle. To validate our findings, we constructed an experimental setup of optical tweezers and demonstrated the enhanced trapping performance of the CPB for larger Mie particles. Moreover, we discovered that, compared to the conventional circular Airy beam with the same focusing length, CPB also presents a significantly better trapping performance. Finally, by adjusting the spatial distribution factor of the CPB, we can effectively control the trapping performance in optical manipulation. The relationship between the trapping force properties of the CPB and the spatial distribution factor can be formulated as an exponential function. Overall, our study provides valuable insights into the optical trapping potential of autofocusing beams, particularly the CPB. These findings open up different avenues for the development of photonic tools in the field of optical trapping and manipulation.

DOI: 10.1103/PhysRevA.108.063509

I. INTRODUCTION

Optical tweezers, introduced by Ashkin in 1986 [1], have been widely utilized across diverse fields such as single molecule biology, biomedicine [2], physics [3], structural assembly of matter [4], and colloidal science [5] due to their contactless and nondamaging micromanipulation properties. Initially, conventional optical tweezers utilized fundamental Gaussian beams (GBs) for trapping. However, as optical tweezer technology has progressed, there is a growing need for precise manipulation and improved photonic tools [6]. Especially, the use of Gaussian beams for manipulating samples in the biomedical field can result in thermal damage, alteration of sample properties, and photodamage due to prolonged light exposure [7,8]. To address these issues, alternative beams such as Bessel beams [9], vortex beams [10], and other structured beams [11–16] have been employed in optical tweezers. These beams generate a toroidal light field structure, reducing the illuminated area, stabilizing trapped optical power, and mitigating photodamage [16]. Researchers continue to work on designing new photonic tools to achieve superior optical trapping performance.

In 2010, the discovery of a circular Airy beam (CAB) sparked significant interest among researchers, leading to the emergence of abruptly autofocusing beams (AAFBs) [17,18]. These beams have unique properties that make them highly valuable in optical tweezers [19]. Unlike Gaussian beams (GBs), AAFBs maintain a low intensity as they propagate, but their intensity rapidly increases, creating a powerful optical trap at the focal points [20]. AAFBs offer distinct advantages for particle manipulation compared to GBs, as they enable precise control at lower power levels, thereby reducing the risk of photodamage. Recently, circular Pearcey beams (CPBs), a type of AAFB, have been studied for their stronger autofocusing properties than CABs, demonstrating an enormous potential for optical manipulations [21,22]. The CPB is a radially symmetric Pearcey beam and emerges from extending the one-dimensional spectrum of the Pearcey beam (Pearcey integral) from Cartesian coordinates to cylindrical ones. Compared to conventional autofocusing beams, such as CABs, CPBs not only achieve abrupt autofocusing at shorter propagation distances but also significantly enhance the focal peak intensity. Additionally, CPBs lack the oscillatory behavior observed in CABs beyond the focal plane. Consequently, the CPB exhibits a substantially stronger trapping force compared to CABs for trapping Rayleigh particles [11]. However, the quantitative characterization of the optical trapping force magnitude of CPB for Mie particle manipulation

*liangyi@gxu.edu.cn

has been relatively unexplored, particularly in experimental studies. Further research in this area is necessary to deepen our understanding of the potential advantages and applications of CPB in optical manipulation and tweezers technology.

Therefore, in this paper, we investigated theoretically and experimentally the autofocusing properties and optical trapping performance of CPB on Mie particles of different sizes. Based on the generalized Lorenz-Mie theory (GLMT) [23–26], we found the CPB exhibits a stronger optical trapping force for a larger Mie particle. In the experiment of trapping particles, the CPB for larger Mie particles always displays a greater trapping stiffness, which indicates the trapping force of the CPB for larger Mie particles is superior. Furthermore, we discovered that, compared to the conventional circular Airy beam with the same focusing length, CPB also presents a significantly greater light intensity, trapping stiffness, and trapping force. Finally, it is found that the relationship between the trapping force properties of the CPB and the spatial distribution factor can be formulated as an exponential function, implying we can flexibly control the trapping performance of CPB by adjusting the spatial distribution factor of the CPB. Our results quantify the optical trapping performance of CPB, which provides a reference for the development of new photonic tools for optical tweezer techniques and biomedical applications.

II. AUTOFOCUSING CHARACTERISTICS OF CPB

In cylindrical coordinates, the electric field distribution of the CPB at the initial plane can be expressed as [21]

$$\Psi(r,0) = A_0\,\mathrm{Pe}\Big(-\frac{r}{S},0\Big)q(r), \tag{1}$$

where A_0 represents the amplitude of the initial spatial field, and Pe denotes the Pearcey integral given by $\mathrm{Pe}(x,y) = \int_{-\infty}^{+\infty}\exp[i(t^4+xt^2+ty)]dt$. The radial distance is described as $r=\sqrt{x^2+y^2}$, where x and y denote the horizontal coordinates. S is the spatial distribution factor employed to control the intensity distribution of the input beam. The function $q(r)$ takes the value 1 for $r \leqslant r_1$, and 0 for $r > r_1$, ensuring limited total power and amplitude distribution of the beam. To investigate the autofocusing and trapping characteristics, we conducted theoretical simulations of CPB propagation using the beam propagation method [27], and observed the propagation process experimentally. For a better comparative analysis, the CPB and circular Airy beam (CAB) were designed to have the same focusing distance at the maximum peak intensity. In our theoretical analysis, we set the parameters as follows: $\lambda = 532$ nm, $S = 80.6$ μm, $r_1 = 0.9$ mm, The incident light power for both beams was maintained at 1 W.

For the experimental investigation, we established the experimental setup [Fig. 1(a)] to examine the propagation characteristics of the CPB and CAB. We employed a semiconductor laser emitting Gaussian beams with a wavelength of 532 nm. The laser beams were collimated and expanded before being incident upon a spatial light modulator (SLM) loaded with holographic phase information. Through a $4f$ imaging system consisting of two lenses, the CPB was generated on the rear focal plane of the second lens. To capture the intensity distribution of the beams at various propagation positions, we utilized charge-coupled devices (CCDs). This facilitated the recording of experimental data and enabled the analysis of the propagation properties of the beams.

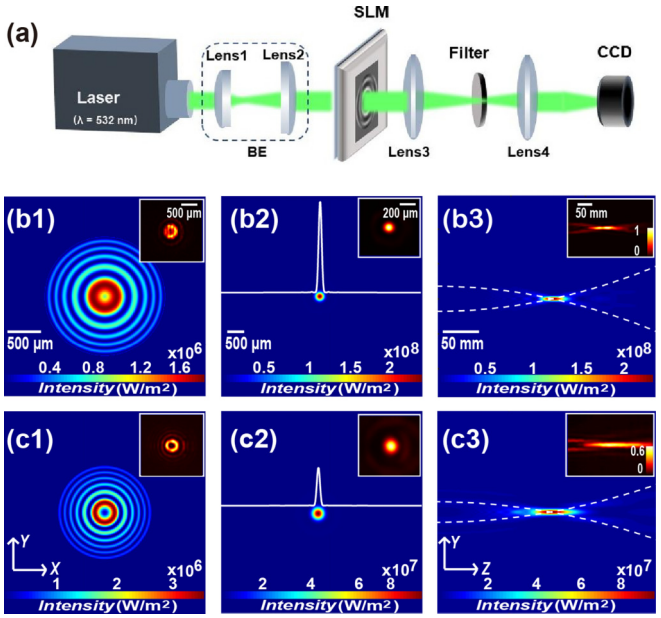

FIG. 1. Propagation of CPB and CAB with the same autofocusing distance ($P = 1$ W). (a) Experimental setup for generating CPB: BE, beam expansion system; SLM, spatial light modulator; CCD, charge-coupled device. (b1) and (c1) are the intensity distributions of the initial position $z = 0$ mm. (b2) and (c2) are the focal positions $z = 150$ mm of CPB and CAB, and the white curve in the middle is the corresponding intensity distribution. (b3) and (c3) are the side views, and the white dashed curve indicates the convergence trajectory of the beams. The illustrations in the upper right-hand corner show the experimental results.

The experimental findings, depicted in Fig. 1, elucidate several noteworthy observations. At the source plane, the light field distribution of the beams aligns with the simulated results, with the innermost ring exhibiting the highest intensity [Figs. 1(b1) and 1(c1)]. The beams achieve autofocusing with a maximum focal peak intensity at $z = 150$ mm [Figs. 1(b2) and 1(c2)]. The peak intensity of the CPB (2.3×10^8 W/m^2) exceeds the initial source light field intensity (1.7×10^6 W/m^2) by more than 100-fold. From a side view [Figs. 1(b3) and 1(c3)], it is evident that the beams exhibit a characteristic intensity distribution during propagation, with a sharp increase of intensity at the focal point followed by a subsequent decrease as they pass through the focus. Comparing the CPB to the CAB, which has the same propagation distance to the maximum peak, the CPB exhibits a larger main ring and fewer additional rings [Figs. 1(b1) and 1(c1)]. Although the initial peak intensities of both beams at the input plane are nearly equal, the autofocusing intensity peak of the CAB (9.3×10^7 W/m^2) is enhanced by only 20 times more compared to the initial source light field intensity (3.4×10^6 W/m^2). Conversely, the CPB generates smaller light spots and demonstrates greater autofocusing ability [Figs. 1(b2) and 1(c2)]. These comparisons substantiate the concurrence between the experimental results and our theoretical predictions.

III. TRAPPING CHARACTERISTICS OF CPB

The distinct autofocusing characteristics of the CPB offer expanded possibilities for particle trapping and manipulation. To further explore its optical trapping force properties on Mie particles (with sizes larger than the wavelength of the incident light), we carried out both theoretical and experimental investigations.

A. Calculation of the trapping force

Theoretically, the Maxwell stress tensor integral and generalized Lorenz-Mie theory (GLMT) [23,24] are utilized to calculate the time-averaged optical force acting on a spherical particle by the beams, and it is denoted as [25,26]

$$F = \oint_s \langle \overleftrightarrow{T} \rangle \cdot \vec{n}\, ds, \tag{2}$$

where $\vec{n}$ is the normal unit vector of the closed surface s around the particle, and the time-averaged Maxwell stress tensor $\overleftrightarrow{T}$ is expressed as

$$\langle \overleftrightarrow{T} \rangle = \tfrac{1}{2}\mathrm{Re}\left[\varepsilon E_t E_t^* + \mu H_t H_t^* - \tfrac{1}{2}(\varepsilon E_t \cdot E_t^* + \mu H_t \cdot H_t^*)\overleftrightarrow{I}\right], \tag{3}$$

where $E_t = E_{\mathrm{inc}} + E_{\mathrm{sca}}$ and $H_t = H_{\mathrm{inc}} + H_{\mathrm{sca}}$ respectively denote the total electric field and the total magnetic field close to the particle. $\overleftrightarrow{I}$ is the unit tensor. Considering the lossless background medium, the three components of the optical force F_x, F_y, and F_z can be simplified to the form expressed by the partial-wave expansion coefficients of the incident and scattered fields [25],

$$F_x = \mathrm{Re}[F_1], \quad F_y = \mathrm{Im}[F_1], \quad F_z = \mathrm{Re}[F_2], \tag{4}$$

where F_1 and F_2 are denoted as

$$F_1 = \frac{2\pi\varepsilon}{\kappa^2}|E_0|^2 \sum_{n,m}\left[c_{11}F_1^{(1)} - c_{12}F_1^{(2)} + c_{13}F_1^{(3)}\right],$$
$$F_2 = -\frac{4\pi\varepsilon}{\kappa^2}|E_0|^2 \sum_{n,m}\left[c_{21}F_2^{(1)} + c_{22}F_2^{(2)}\right]. \tag{5}$$

The expression of the correlation coefficient factors in the above equation are as follows:

$$c_{11} = \left[\frac{(n-m)(n+m+1)}{n^2(n+1)^2}\right]^{\frac{1}{2}},$$
$$c_{12} = \left[\frac{n(n+2)(n+m+1)(n+m+2)}{(n+1)^2(2n+1)(2n+3)}\right]^{\frac{1}{2}},$$
$$c_{13} = \left[\frac{n(n+2)(n-m)(n-m+1)}{(n+1)^2(2n+1)(2n+3)}\right]^{\frac{1}{2}},$$
$$c_{21} = \left[\frac{n(n+2)(n-m+1)(n+m+1)}{(n+1)^2(2n+1)(2n+3)}\right]^{\frac{1}{2}},$$
$$c_{22} = \frac{m}{n(n+1)}, \tag{6}$$

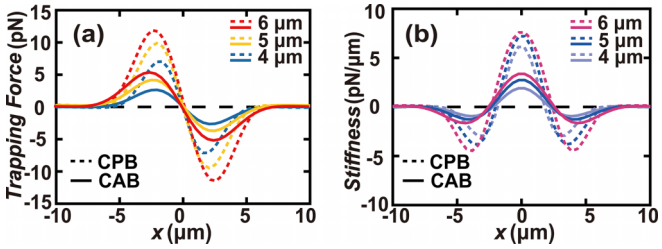

FIG. 2. The optical trapping force and optical trapping stiffness of CPB and CAB at the focal point; (a) is the optical trapping force of CPB (dashed line) and CAB (solid line) for different size particles ($D_s = 4$, 5, and 6 μm) at the focal position; (b) is the optical trapping stiffness (dF/dx) of CPB and CAB for different size particles ($D_s =$ 4, 5, and 6 μm).

and

$$F_1^{(1)} = \tilde{a}_{mn}\tilde{b}^*_{m_1n} + \tilde{b}_{mn}\tilde{a}^*_{m_1n} - \tilde{p}_{mn}\tilde{q}^*_{m_1n} - \tilde{q}_{mn}\tilde{p}^*_{m_1n},$$
$$F_1^{(2)} = \tilde{a}_{mn}\tilde{a}^*_{m_1n_1} + \tilde{b}_{mn}\tilde{b}^*_{m_1n_1} - \tilde{p}_{mn}\tilde{p}^*_{m_1n_1} - \tilde{q}_{mn}\tilde{q}^*_{m_1n_1},$$
$$F_1^{(3)} = \tilde{a}_{mn_1}\tilde{a}^*_{m_1n} + \tilde{b}_{mn_1}\tilde{b}^*_{m_1n} - \tilde{p}_{mn_1}\tilde{p}^*_{m_1n} - \tilde{q}_{mn_1}\tilde{q}^*_{m_1n},$$
$$F_2^{(1)} = \tilde{a}_{mn}\tilde{a}^*_{mn_1} + \tilde{b}_{mn}\tilde{b}^*_{mn_1} - \tilde{p}_{mn}\tilde{p}^*_{mn_1} - \tilde{q}_{mn}\tilde{q}^*_{mn_1},$$
$$F_2^{(2)} = \tilde{a}_{mn}\tilde{b}^*_{mn} - \tilde{p}_{mn}\tilde{q}^*_{mn}. \tag{7}$$

Among them, $m_1 = m+1$ and $n_1 = n+1$, and

$$a_{mn} = a_n p_{mn}, \quad b_{mn} = b_n q_{mn}, \tag{8}$$
$$\tilde{a}_{mn} = a_{mn} - \tfrac{1}{2}p_{mn}, \quad \tilde{p}_{mn} = \tfrac{1}{2}p_{mn},$$
$$\tilde{b}_{mn} = b_{mn} - \tfrac{1}{2}q_{mn}, \quad \tilde{q}_{mn} = \tfrac{1}{2}q_{mn}, \tag{9}$$

where a_n and b_n are the Mie scattering coefficients [28], and p_{mn} and q_{mn} are the partial-wave expansion coefficients of the incident beam. The partial-wave expansion coefficients (a_{mn} and b_{mn}) of the scattered field can be obtained from a_n and b_n, and p_{mn} and q_{mn}, where ε is the dielectric constant in vacuum and $k = 2\pi/\lambda$ is the wave vector.

Based on the above calculation method of optical force, we calculated the optical trapping force of CPB and CAB on polystyrene spheres ($D_s = 4$, 5, and 6 μm) in water. In Fig. 2(a), the optical trapping force exerted on polystyrene beads is depicted at the focal points of the CPB and CAB, with a power of $P = 21.5$ mW. The results illustrate that the optical trapping force of the CPB exhibit an increase in optical trapping force with larger particle sizes [Fig. 2(a), CPB (dashed line)]. Furthermore, the CPB for larger Mie particles always presents a greater trapping stiffness [Fig. 2(b), CPB (dashed line)]. Additionally, the optical trapping force of the CPB is over twice stronger than that of the CAB for three different particle sizes [Fig. 2(a)], and the optical trapping stiffness of the CPB is also more than twice greater than that of the CAB [Fig. 2(b)]. In other words, the CPB demonstrates superior optical trapping capabilities for larger Mie particles. Upon further investigation, the CPB displays enhanced optical trapping capabilities compared to the CAB. This phenomenon arises due to the different autofocusing properties of the two beam types. The CPB exhibits a larger focal peak intensity and a smaller focal point size than the CAB at the same focusing distance. Consequently, the CPB possesses a greater intensity

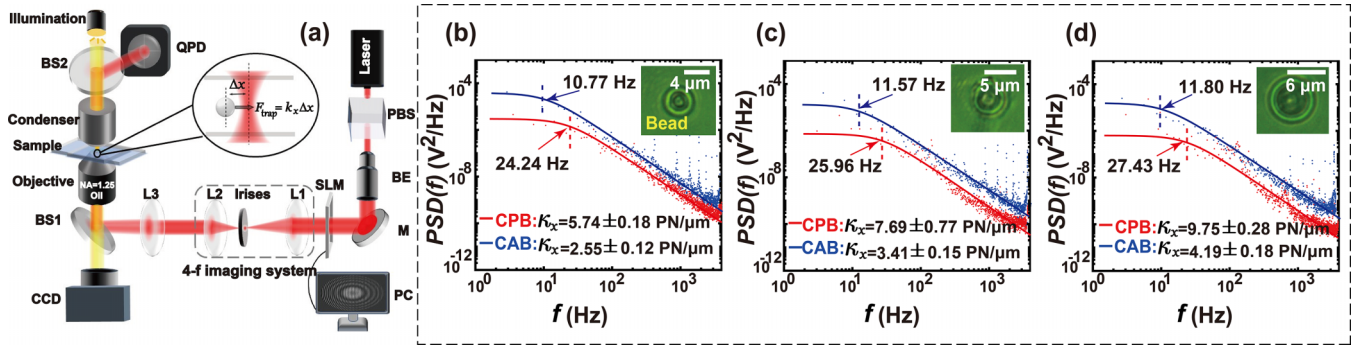

FIG. 3. Experimental schematic diagram for optical tweezers based on autofocusing beams and power spectral density (PSD) of CPB and CAB trapping different sizes of polystyrene beads at a power of 21.5 mW. (a) Laser, $\lambda = 1064$ nm; PBS, polarizing beam splitter; BE, beam expansion system; lens 1 and lens 2 form a $4f$ imaging system; SLM, spatial light modulator; BS, beam splitter; Objective, oil objective (NA = 1.25, 100×); QPD, quadrant photoelectric detectors; CCD, charge-coupled device. (b)–(d) Power spectral density maps of CPB and CAB trapping different sizes of polystyrene beads ($D_s = 4$, 5, and 6 μm) and the illustration in the upper right-hand corner shows polystyrene beads captured. The details of the optical trapping process can be viewed in the Supplemental Material Video [29].

gradient, resulting in a correspondingly higher optical trapping force.

B. Experimental results and discussion

In order to validate the optical trapping performance of the CPB on particles of different sizes in an experimental setting, we constructed CPB-based optical tweezers and compared their trapping characteristics to those of CAB-based optical tweezers. The experimental setup and analytical principles for the optical tweezers are presented in Fig. 3(a). To generate the abruptly autofocusing beams (CPB or CAB), we employed the off-axis hologram method. The hologram was created by interfering the beam wave with a plane wave and loaded onto a spatial light modulator (SLM) using a computer. The laser beam, after passing through a polarizing beam-splitting prism, produced a linearly polarized beam. This beam was expanded by a beam expansion system and then directed towards the SLM. Subsequently, the beams passed through a $4f$ imaging system composed of lens 1 and lens 2. The first-order diffracted light was selected to generate the CPB (or CAB) in free space. Next, the CPB was relayed to the sample using a $4f$ imaging system consisting of lens 3 and an oil lens [numerical aperture (NA) = 1.25, 100×]. By moving the sample stage, the beam acted on the particles, forming an optical trap to capture and hold the particles. Under white light illumination, the trapping of particles was observed using a charge-coupled-device (CCD) camera (the details of the optical trapping process can be viewed in the Supplemental Material Video [29]). The scattered light from the polystyrene beads was collected by quadrant photoelectric detectors (QPDs), which recorded the positional changes of the beads undergoing constrained Brownian motion. This information was further processed using Fourier transform techniques [30,31] to calculate the trapping stiffness.

Accurately, we can obtain the power spectral density (PSD), which has the Lorentzian form and represents the expected value of the average energy in the frequency domain [32]. The power spectrum of particle motion is given by $P(f) = k_B T/[2\pi^2\gamma(f_c^2 + f^2)]$. According to the Langevin equation, the trapping stiffness k_x ($k_x = -dF_{\text{trap}}/dx$) can be calculated from the corner frequency f_c ($f_c = k_x/2\pi\gamma$) of the measured power spectrum. Here, $\gamma = 3\pi\eta D_s$ is the drag coefficient of the trapped particles (given by Stokes' law), k_B is Boltzmann's constant, T is the temperature of the solution, η is the viscosity of the solution, and D_s is the diameter of the object trapped. The optical trapping force of the tweezers can be simply expressed as $F_{\text{trap}} = k_x\Delta x$, since the magnitude of the optical trapping force F_{trap} is proportional to the deviation of the center particle trapped, and the proportionality factor is the optical trapping stiffness. Consequently, the capture capability of different beams can be characterized by the corresponding trapping stiffness.

Figures 3(b)–3(d) display the power spectral density of the CPB and CAB tweezers with an input power of 21.5 mW, while using polystyrene beads as the objects of optical trapping in water. When trapping polystyrene beads with different sizes, it can be observed that the CPB for a diameter of 5 μm exhibits a higher corner frequency f_c (∼25.96 Hz) compared to the diameter of 4 μm (∼24.24 Hz) [Figs. 3(b) and 3(c)]. Using the relation $k_x = 2\pi\gamma f_c$, where γ represents the drag coefficient, the optical trap stiffness of CPB for a diameter of 5 μm is calculated to be approximately 7.69 pN/μm, which is larger than that of the CPB for a diameter of 4 μm (5.74 pN/μm). Similarly, when trapping 6-μm-diameter beads, the CPB demonstrated a higher f_c (∼27.43 Hz) and k_x (∼9.75 pN/μm) [Fig. 3(d)]. This indicates that CPB generates a stronger optical trapping force for larger Mie particles. However, it should be noted that the measured stiffness of the optical trap in the experiment does not precisely match the theoretical predictions. This discrepancy can be attributed to several factors, such as slight differences in the modulation efficiency of the spatial light modulator with finite accuracy for the beams, as well as the imperfection of the experimental setup. We also conducted trapping experiments with CAB on polystyrene beads of different sizes. It was observed that when trapping polystyrene beads with a diameter of 4 μm, the CPB exhibited a higher corner frequency f_c (∼24.24 Hz) and optical trapping stiffness k_x (∼5.74 pN/μm) compared to the CAB, with frequency f_c (∼10.77 Hz) and k_x (∼2.55 pN/μm) [Fig. 3(b)]. Moreover, when trapping 5-μm-diameter beads, the CPB exhibited a higher corner

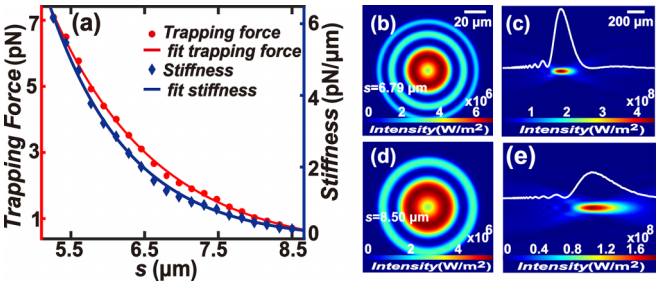

FIG. 4. Optical trapping performance of CPB with different spatial distribution factors for particles ($D_s = 4$ μm). (a) is the changes of optical trapping force and stiffness. (b) and (c) are the initial plane distribution and propagation of CPB at the inflection point of red line in (a) ($S = 6.79$ μm). (d) and (e) are the initial plane distribution and propagation of CPB at the last point of the red line in (a) ($S = 8.50$ μm).

frequency f_c (∼25.96 Hz) and optical trapping stiffness k_x (∼7.69 pN/μm) compared to the CAB, with f_c (∼11.57 Hz) and k_x (∼3.41 pN/μm) [Fig. 3(c)]. Similarly, when trapping 6-μm-diameter beads, the CPB demonstrated a higher f_c (∼27.43 Hz) and k_x (∼9.75 pN/μm) compared to the CAB, with f_c (∼11.80 Hz) and k_x (∼4.19 pN/μm) [Fig. 3(d)]. Evidently, the CPB consistently maintained a greater trapping stiffness than the CAB when trapping polystyrene beads of various sizes, and the trapping stiffness (and consequently the trapping force) increases with an increase in particle size. The experimental observations align with the theoretical calculations based on the full-wave generalized Lorenz-Mie theory and Maxwell's stress tensor method, supporting the conclusion that CPB exhibits superior trapping capabilities for a larger Mie particle. Furthermore, the CPB also presents significantly better trapping capabilities compared to CAB in terms of trapping force and stiffness.

IV. TUNING THE OPTICAL TRAPPING FORCE

Before drawing a conclusion, it is prudent to note that the optical trapping performance of CPB can be further enhanced by selecting an appropriate spatial distribution factor, as indicated by our preliminary numerical simulations. We observed that by modulating the spatial distribution factor of CPB, the optical trapping force and stiffness can be manipulated at the focal point [Fig. 4(a)]. Notably, through fitting and analyzing the calculation results, we discerned that the exponential function $[f(S) = A_1 \exp(B_1 S)]$ accurately depicts the decay process of the optical trapping force and stiffness, where $A_1 = 2.884 \times 10^{-10}$, $B_1 = -7.018 \times 10^5$ in the fitted curve of the force, and $A_1 = 7.83 \times 10^{-4}$, $B_1 = -9.188 \times 10^5$ in the fitted curve of the stiffness. It should be mentioned that as the spatial distribution factor increases, the intensity of CPB decreases, and the size of the focusing spot increases, as evident from analyzing the inflection point and the final point of the trapping force and stiffness [Figs. 4(b) and 4(c) and Figs. 4(d) and 4(e)]. Consequently, this leads to a decrease in the trapping force of CPB at the focal point. Upon closer examination, we discerned that the variation in trapping force was more significant than the intensity under the two spatial distribution factors. This implies that the trapping force is more sensitive to modulation of the spatial distribution factor. In general, by tuning the spatial distribution factor of CPB, we can achieve a greater trapping force for applications in optical tweezers.

V. CONCLUSION

In conclusion, our research substantiates that the autofocusing circular Pearcey beam exhibits a stronger optical trapping force for a larger Mie particle and outperforms circular Airy beams in terms of optical trapping force. By harnessing its superior autofocusing properties and optimizing the spatial distribution factor, CPB exhibits significantly stronger trapping capabilities. These findings have significant implications for the development of advanced optical tweezers with diminished photodamage and enhanced trapping force. The application of CPB holds promise across diverse domains such as biomedicine, colloidal science, and the structural assembly of matter, paving the avenues for innovation in optical manipulation techniques.

ACKNOWLEDGMENT

This work was supported by National Natural Science Foundation of China (Grant No. 11604058), Guangxi Natural Science Foundation (Grant No. 2020GXNSFAA297041).

[1] A. Ashkin, J. M. Dziedzic, J. E. Bjorkholm, and S. Chu, Opt. Lett. **11**, 288 (1986).
[2] H. Xin, Y. Li, Y.-C. Liu, Y. Zhang, Y.-F. Xiao, and B. Li, Adv. Mater. **32**, 2001994 (2020).
[3] H. L. Guo and Z. Y. Li, Sci. China: Phys., Mech. Astron. **56**, 2351 (2013).
[4] X. Chen, L. Lin, Z. Li, and H.-B. Sun, Adv. Funct. Mater. **32**, 2104649 (2022).
[5] S. Pradhan, C. P. Whitby, M. A. K. Williams, J. L. Y. Chen, and E. Avci, J. Colloid Interface Sci. **621**, 101 (2022).
[6] Y. Yang, Y.-X. Ren, M. Chen, Y. Arita, and C. Rosales-Guzman, Adv. Photonics **3**, 034001 (2021).
[7] R. Zhu, T. Avsievich, A. Popov, and I. Meglinski, Cells **9**, 545 (2020).
[8] Y. Xie and X. Liu, J. Biophotonics **15**, e202100315 (2022).
[9] Y. A. Ayala, A. V. Arzola, and K. Volke-Sepulveda, J. Opt. Soc. Am. B **33**, 1060 (2016).
[10] L. Tan, N. Liu, F. Lu, D. Liu, B. Yu, Y. Li, H. Wu, K. Chen, Y. Chu, P. Hong, and Y. Liang, Phys. Rev. A **107**, 043501 (2023).
[11] Y. Liang, L. Tan, N. Liu, K. Chen, H. Liang, H. Wu, B. Luo, F. Lu, H. Chen, B. Zou, and P. Hong, Phys. Rev. Appl. **19**, 014016 (2023).
[12] F. Lu, L. Tan, Z. Tan, H. Wu, and Y. Liang, Phys. Rev. A **104**, 023526 (2021).

[13] C. He, Y. Shen, and A. Forbes, Light: Sci. Appl. **11**, 205 (2022).
[14] A. I. Bunea and J. Gluckstad, Laser Photonics Rev. **13**, 1800227 (2019).
[15] F. Lu, H. Wu, Y. Liang, L. Tan, Z. Tan, X. Feng, Y. Hu, Y. Xiang, X. Hu, Z. Chen, and J. Xu, Phys. Rev. A **104**, 043524 (2021).
[16] E. Otte and C. Denz, Appl. Phys. Rev. **7**, 041308 (2020).
[17] D. G. Papazoglou, N. K. Efremidis, D. N. Christodoulides, and S. Tzortzakis, Opt. Lett. **36**, 1842 (2011).
[18] I. Chremmos, N. K. Efremidis, and D. N. Christodoulides, Opt. Lett. **36**, 1890 (2011).
[19] Y. Jiang, Z. Cao, H. Shao, W. Zheng, B. Zeng, and X. Lu, Opt. Express **24**, 18072 (2016).
[20] I. Kaminer, M. Segev, and D. N. Christodoulides, Phys. Rev. Lett. **106**, 213903 (2011).
[21] X. Chen, D. Deng, J. Zhuang, X. Peng, D. Li, L. Zhang, F. Zhao, X. Yang, H. Liu, and G. Wang, Opt. Lett. **43**, 3626 (2018).
[22] J. D. Ring, J. Lindberg, A. Mourka, M. Mazilu, K. Dholakia, and M. R. Dennis, Opt. Express **20**, 18955 (2012).
[23] G. Gouesbet and G. Grehan, J. Opt. A: Pure Appl. Opt. **1**, 706 (1999).
[24] G. Gouesbet and G. Gréhan, *Generalized Lorenz-Mie Theories* (Springer, Berlin, 2011), pp. 37–88.
[25] W. Lu, H. Chen, S. Liu, and Z. Lin, Opt. Express **25**, 23238 (2017).
[26] Q. Ye and H. Lin, Eur. J. Phys. **38**, 045202 (2017).
[27] S. Yoneta, M. Koshiba, and Y. Tsuji, J. Lightwave Technol. **17**, 2398 (1999).
[28] C. F. Bohren and D. R. Huffman, *Absorption and Scattering of Light by Small Particles* (Wiley, New York, 1998), pp. 82–129.
[29] See Supplemental Material at http://link.aps.org/supplemental/10.1103/PhysRevA.108.063509 for details of the optical trapping process.
[30] K. Berg-Sørensen and H. Flyvbjerg, Rev. Sci. Instrum. **75**, 594 (2004).
[31] P. H. Jones, O. Marago, and G. Volpe, *Optical Tweezers: Principles & Applications* (Cambridge University Press, Cambridge, UK, 2015).
[32] J. Gieseler, J. R. Gomez-Solano, A. Magazzù, I. P. Castillo, L. P. García, M. Gironella-Torrent, X. Viader-Godoy, F. Ritort, G. Pesce, A. V. Arzola, K. Volke-Sepúlveda, and G. Volpe, Adv. Opt. Photonics **13**, 74 (2021).